

https://dspace.org/

Radiolysis of water by and particles from spent nuclear fuel

Mosebetsi Leotlela

PERGAMON-ELSEVIER SCIENCE LTD
https://hdl.handle.net/10539/40885
WOS

Downloaded from a DSpace repository. https://dspace.org/

Radiation Physics and Chemistry 216 (2024) 111361

Contents lists available at ScienceDirect

Radiation Physics and Chemistry

journal homepage: www.elsevier.com/locate/radphyschem

Radiolysis of water by α- and β-particles from spent nuclear fuel

M.J. Leotlela

School of Physics, University of the Witwatersrand, Johannesburg, South Africa

ARTICLE INFO

Handling Editor: Dr. Chris Chantler

Keywords:
Redox reaction
Nanotechnology
Hydrogen energy
Free radicals
Linear energy transfer
G-values

ABSTRACT

When water is subjected to radiolysis by charged ionising radiation particles (β and α-particles) from nuclear plants, they generate H_2 as one of the radiolytic byproducts which has highest Gvalues than other radiolytic products. The Gvalues obtained by α-radiolysis used are listed in brackets next to their respective nuclides which are: ^{237}Np (2.551E−01), ^{241}Am (2.269E−01), ^{242m}Am(2.370E−01). In addition to a high Gvalue, it also has high calorific value (141 MJ/kg) which can be used in hydrogen energy generation (HEG). Hence, apart from the radiological health risk of nuclear plants, if H_2 released nuclear plants is harvested and used in hydrogen energy generation it can result in great cogeneration opportunities where nuclear energy supplies hydrogen, which would otherwise be wasted, to a hydrogen energy generation plant for additional power generation.

This is even more advantageous if one takes into consideration that hydrogen Gvalues (G(H)) values from nuclear plants increase with an increase in duration of water exposure to ionising radiation and also that it, i.e. (G(H)values also increase with an increase in radiation flux to which water is exposed. Hence the longer the nuclear plant is running and the higher the power reactor is increased (and consequently the radiation flux) the higher the Gvalues of hydrogen and therefore the higher the power output of hydrogen energy generation.

The idea of cogeneration becomes even more lucrative if we consider that hydrogen energy generation is clean (also known as green energy) because of its insignificant contribution to environmental pollution. Therefore, as energy demand increases and the need to curb climate change by reducing over reliance on power generation that release large quantities of CO_2 to the atmosphere is heightened; the more sense it makes from energy generation/supply and environmental protection point of view for cogeneration of hydrogen energy and nuclear energy.

This article presents the results of radiochemical events/processes that occur when water is exposed to ionising radiation of charged particles (β and α-particles). These results supplement the fluctuation in effective dose theory/hypothesis of a previous study on time-dependent variations in the radiological health impact of an interim SNFS facility presented in 2021 (Leotlela, 2021). It also provides an analysis of factors that cause radiation damage by studying the effects of the dose rate on both high and low linear energy transfers (LETs). High LET radiation refers to all those particles with a track-average LET higher than a few eV nm^{-1}. These include alpha particles, protons, neutrons, and heavy ions. Low LET, on the other hand, refers to particles with a track-average LET lower than 1 eV nm^{-1}. These include beta, gamma, x-rays and electrons.

1. Introduction

In a research article published in 2021, it was discovered that the radiation dose from interim spent fuel is time dependent (Leotlela, 2021; Basheer & Ali, 2019; Baldacchino et al., 2019). Some factors that were cited as the cause of fluctuations were the energy of particles, the probability of emission and, in the case of neutrons, the number of neutrons emitted per fission ($\bar{\nu}$) (Leotlela, 2021).

Other factors that have been reported by other researchers as fluctuating are the radiolysis species/by-products emanating from the exposure of biological cells[1] to radiation, which often do not receive the same prominence in industrial safety, be it radiation or chemical safety,[2] as the radiation exposure that caused/generated them. In radiation safety the emphasis is often on radiation protection, which is the first line of defence in preventing the health effects of radiation exposure. However, after the cell is exposed to radiation there is a sequence of

E-mail address: mosebetsi.leotlela@wits.ac.za.

[1] In radiolysis this is often represented by water molecules because human tissue is made of 60–70% water.

[2] Safety from harmful chemical products.

https://doi.org/10.1016/j.radphyschem.2023.111361
Received 2 June 2023; Received in revised form 26 September 2023; Accepted 23 October 2023
Available online 4 November 2023
0969-806X/© 2023 The Author. Published by Elsevier Ltd. This is an open access article under the CC BY-NC-ND license (http://creativecommons.org/licenses/by-nc-nd/4.0/).

physico-chemical processes which are both physical and chemical in nature. These are beyond the scope of radiation protection and often lead to the breakdown of water molecules (Dzaugis et al., 2015). This (i.e. the breakdown of the water molecule) is often the beginning and the major cause of radiation-induced health effects because radiation exposure gives rise to a number of reducing and oxidising agents (REDOX) which are corrosive in nature and will consequently subject a cell to severe oxidative stress (Bielski et al., 2009).

The concentration of the primary yields of radiolysis products is dependent on the type of particle (α-, β-, or γ-rays or neutrons) that interacts with the target material and its energy (i.e. the energy of the projectile). In this study, the mathematical relation between the dose rate *and* the linear energy transfer (LET) *and* between the LET and the distance of interaction are presented. The study evaluated the role of radiation dose *and* the effect of oxidation–reduction reaction in a tissue with a view to determining their impact on the G-values of various radiolysis products (Leotlela, 2021).

1.1. Application of ionising radiation in hydrogen energy generation

One of the spinoffs of radiolysis as indicated in the body of the text of this paper is production of hydrogen which can be used in hydrogen energy generation because of its high heating value (141 MJ/kg) (Ali and Basit, 1993; Ali et al., 2022). This is quite a significant finding considering that there is already worldwide demand for high energy production given that demand already exceeds supply[3] and also considering that based on the estimation of energy consumption statistics it is projected that fossil fuel i.e. coal natural gas and oil are gradually being depleted and according to projections they will only last for about 150 years (Jawhari, 2022). It is therefore important that an alternative energy source is found and over reliance on CO_2 emitting energy sources is decreased. Considering that hydrogen energy is a clean form of energy and has high calorific value, it would therefore be a logical thing that more investment is made towards the research of hydrogen energy generation and storage.

Many researches in hydrogen production conducted so far are focussing on production of hydrogen using non-ionising radiation such as UV radiations, visible light, infra-red radiation, and X-radiation. Although these do achieve the goal, the hydrogen from these sources have low hydrogen Gvalues and therefore are not efficient techniques of radiolysis for hydrogen energy generation on an industrial scale (Ali, et al., 2022; Ali et al., 2023). Thus, given hydrogen is already one of the byproducts in nuclear plants which is not used, it is imperative that an innovative way of co-generation is developed where the hydrogen which is emitted from nuclear reactors is channelled to hydrogen energy generation as this reaction shows $\{2H_2(gas) + O_2(gas) = 2H_2O + energy\}$ instead of being lost as waste gas (Najjar and Safadi, 2016).

1.2. The role of advanced materials for hydrogen energy generation

The rate at which radiochemical reaction occurs (and subsequently the yield of radiolytic byproducts) and the amount that can be stored can greatly be increased if proper selection of material are used as catalysts and as storage medium (Armstrong et al., 2013). Thus, knowledge of new emerging technologies in alternative energy generation and their storage is of great importance.

Most common material being researched for hydrogen fuel storage and catalyst for hydrogen generation are nanomaterials which Christian et al. define as "*particulate matter with at least one dimension that is less than* 100 nm" (Christian, et al., 2008; Heera and Shanmugam, 2015), while the US Food and Drug Administration (USFDA) defines them as "*materials that have at least one dimension in the range of about 1 to* 100 nm *and show dimension-dependent behaviour*" (Singh et al., 2023).

[3] As witnessed by the number and duration of load shedding in South Africa.

There are many ways in which nanomaterials are classified but for the purpose of this article the classification that will be adopted is one that classify them into the following categories; inorganic nanoparticle, polymeric nanoparticles, solid lipid nanoparticles, liposomes, nanocrystals, nanotubes, dendrimers (Heera and Shanmugam, 2015; Singh et al., 2023).

i. Characteristic of nanoparticles:
   a. *Nanoparticle structure and composition*: they can be made of a single material or may be made a composite of more complex material.
   b. *The surface of nanoparticles*: they may be made up of metal ions, small molecules, surfactants, polymers.
   c. *The shell*: The outer layer is made of material that is different from that of the core and therefore considered to be a shell.

ii. Properties of nanoparticles: the fate and behaviour and consequently thus their functionality and application of nanoparticles as well as their effectiveness where they are used is defined by their properties. Some of their properties are;
   a. *Particle mobility*: this aspect is a function of a number of factors like diffusion, buoyancy, Brownian motion. The interrelationship among these factors is described by the Einstein-Stoke law of diffusion which Christian et al. (2008) defined as $Df = kT$ where D is the diffusion coefficient, k is Boltzmann constant and T is the temperature, and f is the frictional coefficient defined by $f = 6\pi\eta a$, where, η = the velocity of the medium, a = particle radius,
   b. *Surface energy and colloidal stabilisation*: generally, small and light nanoparticles would form a stable suspension of the medium under steady state. If however, the suspension is swirled, that will destabilize the charge orientation and polarity of adjacent magnetic nanoparticles and subsequently of the entire colloid. Because of that they would agglomerate and form a sediment at the bottom of the vessel. To prevent this, the design of nanoparticles includes a layer that separates adjacent nanoparticles so as to keep the electric charge distribution and polarity unaffected by change in steady state (Leotlela et al., 2020b).
   c. *Morphology*: Morphology of nanoparticles may be classified as either; spherical, circular, convex or they may be described by their aspect ratio (Leotlela, 2019).
   d. *Catalysis*: The effectiveness of nanoparticles as catalysts if defined by the ration of the surface area to volume; the larger the surface area available for reaction the better is the catalytic effect.

Thus, the container/substrates of the redox solution is not just a "spectator" in the chemical reaction, it is actively participating in the chemical reaction as a catalyst (Buettner, 1992; Katsumura et al., 2020). The degree of effectiveness of participation depends on the contact area available for the reaction, material composition e.g. energy band.

The novelty of this work is in radiolysis of water with *charged particles*. It also highlights the application of ionising radiation from nuclear reactors in hydrogen generation which hasn't been considered so far as the focus of much research has been on non-ionising radiation.

2. Materials and methods

The simulations were performed using the alpha dose rate calculator (ADRC) and where necessary the results were verified by developing a computer program using python program to verify that they were reproducible (cf Appendix 1) (Anaconda Inc, 2023) (Kloss, 2009). The ADR is a computational model developed for calculating the dose rate of a planar alpha-emitting surface with high efficiency. It is based on the same techniques and principles as the Stopping Ranges of Ions in Matter (SRIM) software where the stopping range data of a projectile in a medium is analysed. The accuracy of the results from ADRC have been found to replicate those obtained using Monte Carlo N-Particle (MCNP) code (Sibery, 2020; Kirkegaard, 2008).

The materials used in the cask under study are listed in Table 1

Table 1
Materials used in the cask (Leotlela, 2016; Leotlela et al., 2017).

Material no.	Material	Description	Purpose
0	void	Gap	To provide ventilation
1	UO_2	Nuclear fuel	Nuclear fuel for fission purposes which, in addition to many other nuclides, is made of these actinides, with their respective percentage contribution in weight (%) in brackets:^{234}U(0.04) ^{235}U (3.25%), ^{236}U(0.02), ^{238}U(69.96), where the percentage of UO2 indicates enrichment. During the operation of the reactor, there is an increase in fission products (cf. (Leotlela et al., 2017) and other actinides which include ^{238}Pu, ^{239}Pu, ^{240}Pu, ^{241}Pu and ^{241}Am.
2	Zirc-2	Zirconium alloy	Fuel cladding
4	B_4C–Al_2O_3	Alloy of boron carbide and aluminium oxide	Neutron absorber
5	Stainless steel 304 (SS-304)	Metal frame of the cask	To provide structural support and strength to equipment. It has the following composition (wt %); Mn (2.0), Fe (69.5), Ni (10.5), Cr (18). The iron (Fe) in the composition of SS-304 also plays a role in redox reaction.
6	Borated steel	An alloy made up of steel and boron	Steel with the following composition in wt% in brackets: B(0.9), Si (1),Mn (2), Fe(67.1),Ni(10), Cr (19). Boron (B) is enriched with enriched with ^{10}B to effect better neutron absorption.
8	H_2O	Water	Water is normally not used in dry casks; however, water is included in this project to (1) emulate the biological cell/tissue and enable radiolysis in an aqueous medium; and to (2) act as a neutron shield.
9	Polyethylene	Polyatomic hydrocarbon	Because of its high percentage of hydrogen atoms, it is included in the design of the cask to act as radiation shielding material which it does mainly by scattering the fast neutrons.
10	Cast iron	Metal frame of the cask	Consists of Mn (0.6), Si (1.96), Fe (92.63), carbon graphite (3.5), Ni (1.31). The purpose is to provide strength and structural support, as well as corrosion resistance support
13	Dry air	Gas which can be either argon or nitrogen	To provide an inert environment and to act as a coolant
14	Regular concrete (cf. Fig. 1 for a concrete slab)	Concrete slab	Concrete slab to provide mechanical stability against vibrations from earthquakes; built at least 1 m above the ground to minimise radiation exposure of members of the public.

(Leotlela et al., 2020a,b; Leotlela, 2021).

The α-source nuclides listed in Table 2 and their respective energies, at a specific activity of 500 kBq/g and a γ-background dose rate of 10 Gy/s, were used in the simulations (Sibery, 2020; Butarbutar et al., 2014).

The pore radius used in the simulation was 1 μm, and the fuel was simulated as being surrounded by water (Sibery, 2020). The casks under study were arranged in a vertical position, as in Fig. 1, and to effect radiolysis the simulation was performed with casks flooded with theoretically chemically pure water i.e., the chemical composition was H_2O, no other impurities (Leotlela, 2021; Leotlela et al., 2017; Leotlela et al., 2020a; Leotlela et al., 2020b; Yoshikawa et al., 2000). Measurements of the dose rate were taken at a distance of approximately 10 m from the SNFS co-ordinates [(x, y, z) = (3.66, 1029.24, 49.00)], which is the public exclusion boundary (Leotlela et al., 2020a,b).

3. Results

3.1. Radiolysis by α-particles

As a particle diffuses through a medium with which the fissile vessel is filled, it interacts with nuclei of the target material and transfers some of its excess energy to the nuclei of the medium per unit length traversed (dE/dx).[4] Because of that it is important for one to determine the nature of the relationship between the distance traversed and the LET and between the LET and the dose rate (Baiocco et al., 2016; Baldacchino et al., 2019).

The results in Fig. 2 indicate that when water is irradiated with α-particles, the relationship between the dose rate and the distance from the interface follows an exponential decay described by Eqn (1), and the values of the respective parameters in Eqn (1) and their uncertainties are listed in Table 3.

$$y = y_0 + Ae^{-x/t} \quad \text{Eqn 1}$$

where.

y_0 = the offset
A = amplitude, and
t = decay constant.

Regarding the relationship between the LET and the distance from the interface, the results illustrated in Fig. 3 indicate that there is a non-

Table 2
Nuclides used in high-LET analyses.

Radionuclide	Energy (MeV)
^{241}Am	5.479
^{242m}Am	5.208
^{237}Np	4.768
^{238}Pu	5.487
^{239}Pu	5.148

[4] Also known as LET.

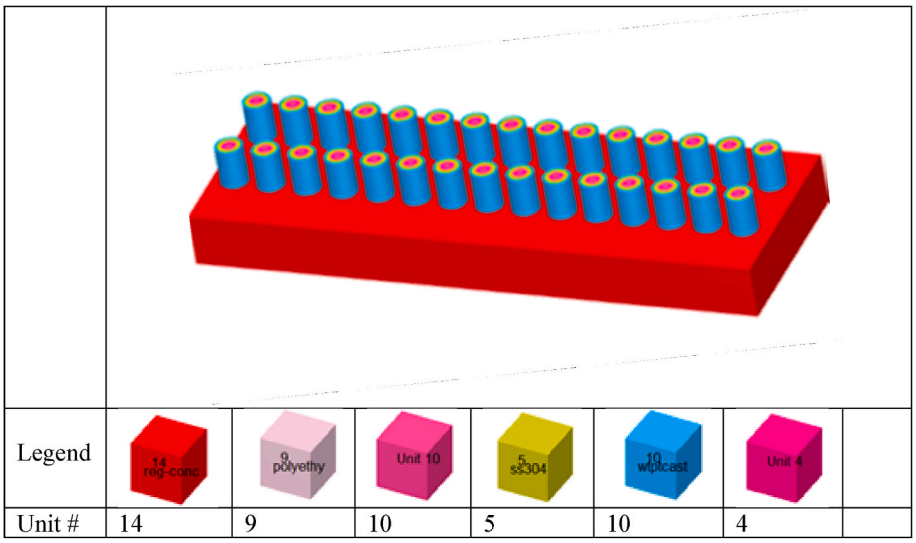


Fig. 1. Interim spent fuel storage facility with a 2 × 15 storage matrix (Leotlela, 2021).

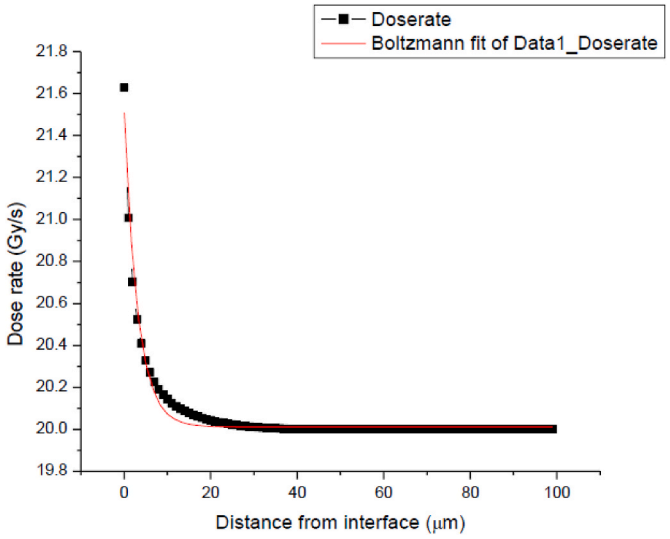


Fig. 2. The dose rate as a function of the distance from the interface for α-particle interaction.

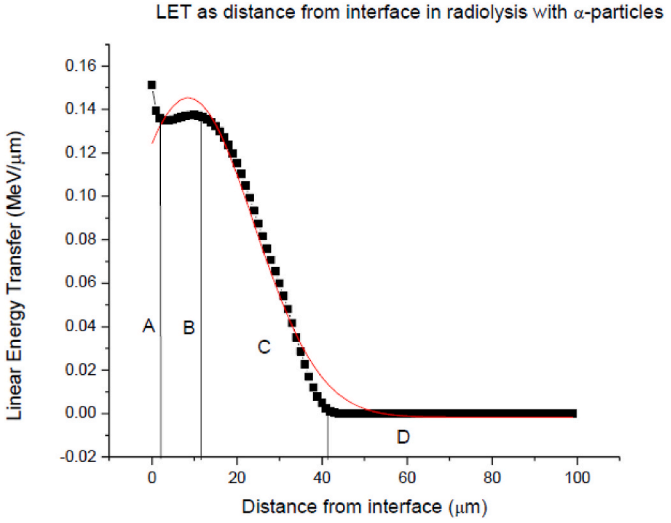


Fig. 3. LET as a function of the distance from the interface in radiolysis with α-particles.

Table 3
Values for the parameters used in the Boltzmann equation for the dose rate versus the distance from the interface for radiolysis with α-particles.

Parameter	Value	Δ (±)
y_0	20.01131	0.00329
A	1.498	0.02611
t	3.14124	0.09312

linear correlation between LET and the distance from the interface.

This (i.e., the relationship between LET and the distance from the interface) may be summarised mathematically by Eqn (2). The parameters applicable to Eqn (2) and their respective values that were found to be a perfect fit for this equation, i.e. Eqn (2), are listed in Table 4.

$$y = y_0 + \frac{A}{w\sqrt{\pi/2}} e^{-2\frac{(x-x_c)^2}{w^2}}, \qquad \text{Eqn 2}$$

where.

Table 4
Values of parameters in the equation of LET versus the distance from the interface, i.e., Eqn (2) in α-radiolysis.

Parameter	Value	Δ(±)
y_0	−0.00177	0.00079
xc	8.57309	0.36887
w	30.85135	0.72198
A	5.69248	0.14014
χ2/DoF	R^2	
0.00003	0.99041	

y_0 = off-set
x_c = centre
w = width, and
A = area.

The analysis proved that when the values in Table 4 are applied to their respective parameters, the results are $R^2 = 0.99041$ and $\chi^2/\text{DoF} = 0.00003$.

The response of LET to the interaction distance, as depicted in Fig. 3,

may be described well if the figure is divided into the following regions.

- **Region A**: from 0.08 to 2.079 μm: *There is a steep decrease in* LET *that may be ascribed to the fact that the target/substrate is new/fresh, does not have imperfections and still has its original density and its original crystal or chemical structure. Because the unit cell has a high density relative to a unit cell that has already suffered radiation damage, when the α-particle diffuses through the medium, it experiences a high intensity/frequency of interaction with the nuclei of a target material. Because of this high intensity of interaction, the particle loses some of its energy to the nuclei of the target material. The* LET *will, therefore, decrease much more rapidly in the earlier stages of diffusion and the interaction distance, hence a steep* LET *in the first few μm.*
- **Region B**: from 2.079 to 10.412 μm: *The target material has undergone radiation damage and experienced an increase in atomic vibrations because of the earlier interaction. Because of that, the atoms of the unit cell of the target material are further apart; therefore, an α-particle diffusing through this material will experience a low interaction frequency than that in region A, resulting in a lower* LET per *path length and thus an increase in the* LET.
- **Region C**: between 10.412 and 40.838 μm: *There is a rapid decrease in the* LET, *albeit at a lower rate than that in A. The decrease in the* LET *in B relative to that in A may be ascribed to the fact that in B, the cell structure was not completely destroyed; consequently, the structure has managed to repair itself but not to the same condition as it originally was in A. Because of that, the cell density and chemical structure have somewhat been restored enough to provide an increased frequency of interaction between α-particle projectiles and the target material compared to that in B, and because of this, i.e. increased frequency of interaction, the alpha particle loses its energy much quicker than in B, even though slower than in A; that is why there is a decrease in the LET.*
- **Region D**: beyond 40.838 μm: *The cell structure is completely destroyed to such an extent that atoms of the unit cell are so far apart, and the density of the unit cell so low that the frequency of interaction is also very low. If the atoms do interact at all, they may only be making a glancing collision that only results in excitation of the atoms; therefore, LET increases asymptotically with the increase in the interaction distance.*

As illustrated in Fig. 4, the results of this study indicated the LET as a function of the dose rate to which the medium is exposed. Furthermore, the analysis also revealed a non-linear relationship between the LET and the dose rate from α-particles, described mathematically by Eqn (3). The values for the parameters applicable to Eqn (3) in the case of the dose rate versus the LET in α-radiolysis are listed in Table 5.

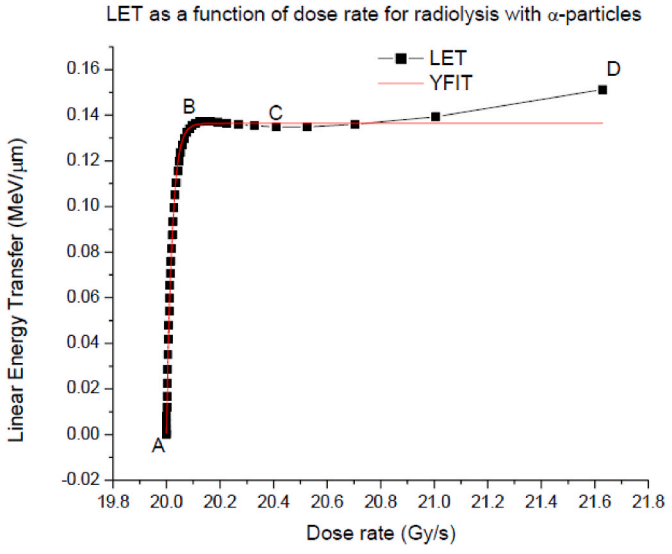


Fig. 4. LET as a function of the dose rate for radiolysis with α-particles.

$$y = \frac{A_1 - A_2}{1 + e^{(x-x_0)/dx}} + A_2 \qquad \text{Eqn 3}$$

Further to confirming the relationship between the dose rate and the LET, an analysis was conducted to determine the relationship between the energy of α-particles emanating from nuclides together with the respective G-values of radiolysis products. The results in Table 6 indicate that the G-values from nuclides are functions of the average dose rate over the layer through which the α-particles diffuse.

By varying the duration of exposure, the time-dependent G-values in Fig. 5 were obtained. The results indicate a direct linear relationship between G-values and exposure time such that the yields of H_2 and H_2O_2 occur at much higher rate than that of other radiolysis products.

3.2. Radiolysis by β-particles

For low-LET analysis, water was irradiated with β-particles from UO_2 fuel in which the nuclides listed in Table 7 were run/simulated simultaneously and in isolation from one another.

The results indicate that the relationship between the dose rate and the distance of interaction may be represented by Fig. 6, which obeys Eqn (3).

$$y = y_0 + Ae^{-x/t}, \qquad \text{Eqn 4}$$

where.

y_0 = off-set
A = amplitude, and
t = decay constant.

The values for parameters in Eqn (4) and their respective uncertainties are listed in Table 8.

With regard to the relationship between LET and the distance from the interface with β-particles, the results prove that the relationship is as depicted in Fig. 7.

It has also been established that this relationship may also be described by Eqn (3) for radiolysis with β-particles, except that its parameters and their respective values and uncertainties are now as listed in Table 9.

The results of the interpretation of the parameters applicable to Eqn (3), as used with reference to the LET–distance graph for radiolysis with β-particles, are listed in Table 9 and illustrated pictorially in Fig. 7.

The study further showed that the relationship between dose rate and LET may be represented by Fig. 8, which is described mathematically by Eqn (3) with values listed in Table 10.

Regarding the effect of temperature on the production rate of various radiolysis products, the results indicate that for any given radiolysis product (e.g. $e_{(aq)}$), its G-value does not respond in the same manner when water is exposed to high (Hi) LET as when it is exposed to Lo LET (Katz and Cucinotta, 1991; Kentaro, 2021). Evidence for this is provided in Fig. 9, which illustrates the response of various G-values to a temperature increase.

Table 5
Values of the parameters of Eqn (3) when applied in the analysis of the dose rate versus LET in case of α-radiolysis.

Parameter	Value	Δ (±)
Initial Asymptote (A_1)	−2.1867	3.45
Final Asymptote (A_2)	0.13644	6.11E−04
x at y50 (x_0)	19.945	0.0348
Width(dx)	0.019923	0.00125
x at y20	19.91703	
x at y80	19.97227	
X^2/DoF	5.44E−06	
R^2	0.9983	

Table 6
G-values for various radiolysis products that resulted from radiolysis by respective nuclides at 1000 decays.

	Radiolysis product	^{241}Am	^{242m}Am	^{237}Np	^{238}Pu	^{239}Pu
G-values (μmolL^{-1}) at 25 °C	H_2	2.269E−01	2.370E−01	2.551E−01	2.268E−01	2.396E−01
	H_2O_2	1.838E−01	1.920E−01	2.067E−01	1.837E−01	1.941E−01
	$e_{(aq)}$	1.767E−02	1.846E−02	1.987E−02	1.837E−01	1.866E−02
	H (rad)	1.838E−02	1.920E−02	2.067E−02	1.766E−02	1.941E−02
	OH (rad)	6.431E−02	6.719E−02	7.233E−02	6.429E−02	6.792E−02
	HO_2 (rad)	1.838E−02	1.920E−02	2.067E−02	1.837E−02	1.941E−02
	H^+	3.308E−02	3.455E−02	3.720E−02	3.306E−02	3.493E−02
	Average decay energy (MeV)	5.479E+00	5.208E+00	4.768E+00	5.487E+00	5.148E+00
	Average dose rate over diffusion layer (Gy/s)	5.890E−03	6.153E−03	6.624E−03	5.887E−03	6.220E−03

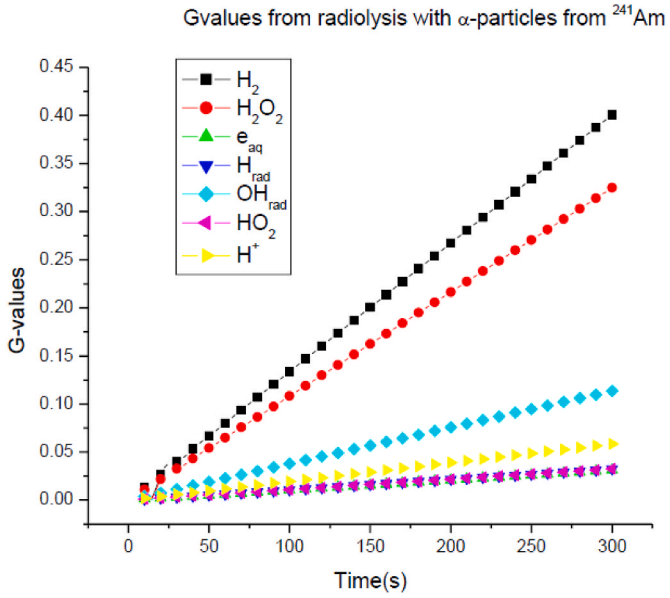


Fig. 5. G-values as functions of exposure duration for α-induced radiolysis from ^{241}Am.

Table 7
Nuclides taken into consideration for LET resulting from β-particles.

Radionuclides	Average energy (MeV)
^{241}Pu	0.005
^{239}Np	0.115
^{137}Cs	0.171
^{85}Kr	0.251

These results have been found to be comparable with those published by Sibery (2020).

3.3. Effects of oxidation-reduction properties of actinides in radiolysis

The importance of redox reaction from actinides in effecting radiation damage because of the radical pairs they give rise to will be demonstrated by the interaction of radiation with (1) biological cells/tissue such as the deoxyribonucleic acid (DNA) because of its sensitivity to radiation and (2) the material out of which various components of the fissile systems are constructed from such as UO_2 fuel pellet and other material. These materials are used to study the underlying factors that lead to the degradation of material exposed to radiation in the presence of water because of possible ground water incursion during storage. This will give both a biological and a material physics/engineering perspective on the redox reaction of actinides.

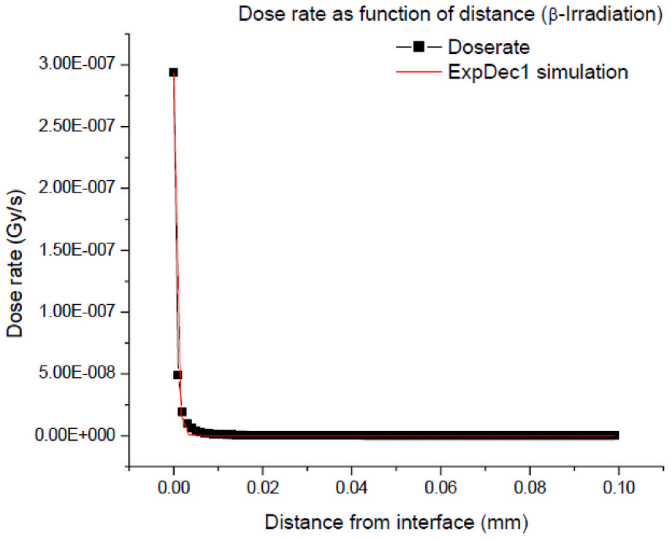


Fig. 6. Dose rate as a function of the distance of interaction (β-irradiation).

Table 8
Values for parameters used in the dose rate–distance mathematical relation for β-radiolysis (Eqn (4)).

Parameter	Value	Δ(±)
y_0	0	0
A_1	2.94E−07	1.58E−09
t_1	0.00059	9.70E−06
X^2/DoF	R^2	
2.50E−18	0.99721	

3.3.1. Implications for radiation biology

When a biological cell is exposed to radiation the α-particles react with the DNA to generate a number of radiolytic products which include $^1O_2$, OH, H_2O_2, NO and hydroxyl radical, collectively known as reactive oxygen species (ROS). The accumulation of these to abnormal quantities which the cell cannot regulate causes oxidative stress in the cell, often with severe health effects, for example many types are as a result of inflammation and a high level of ROS (Tretter et al., 2022). To compare the efficiency of different radiations in causing cell damage resulting from oxidative stress, radiobiological effectiveness (RBE) (Yoshikawa et al., 2000) is applied, which is defined by Eqn (5).

$$RBE = D_{ref}/D_{test} \quad \text{Eqn 5}$$

where D_{ref} is the biological effect of a reference dose and D_{test} is the biological effect of a test dose (Butarbutar, 2014; Ford et al., 2001; Katz and Cucinotta, 1991).

Iron is an important component cell because it is vital in metabolism, oxygen transport, DNA synthesis. However, its amount is regulated not to exceed the limit as it tends to for free radicals in the oxidation-

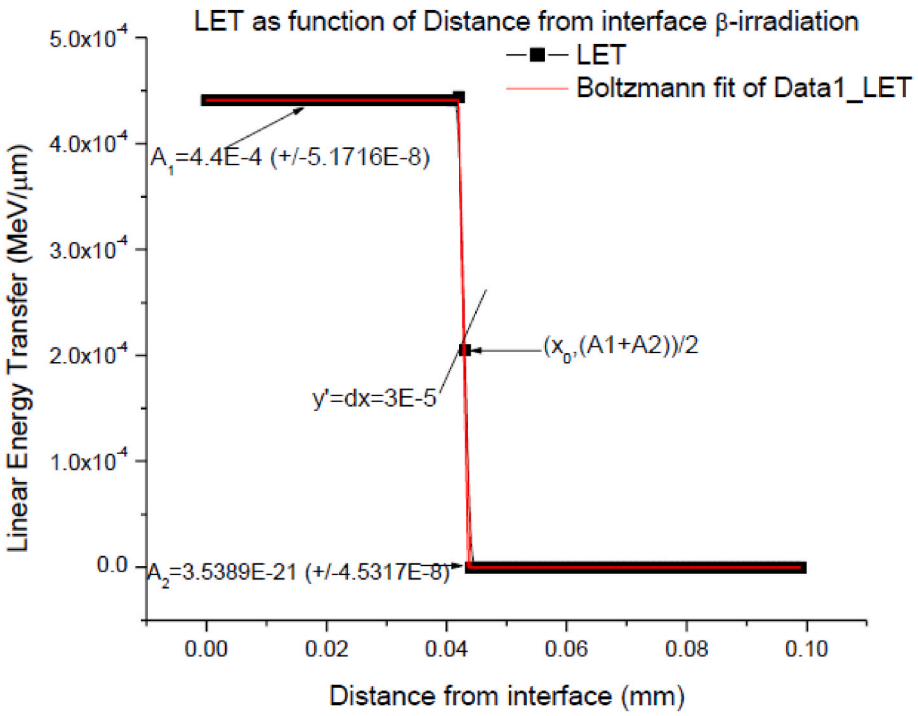


Fig. 7. LET as a function of the distance from the interface (β-particles).

Table 9
Data for parameters used in the LET–distance graph for radiolysis with β-particles.

Parameter	Value	Δ (±)
Initial Asymptote (A_1)	0.00044	5.17E−08
Final Asymptote (A_2)	3.54E−21	4.53E−08
x_0 = x at y50	0.043	4.48479
dx	0.00003	32.18498
x at y20	0.04293	
x at y80	0.04306	
χ2/DoF	R^2	
1.15E−13	1	

Table 10
Values for parameters in the equation for LET versus the dose rate for radiolysis using β-particles.

Parameter	Value	Δ(±)
A_1	−2.65E−14	
A_2	0.00044	5.17E−08
x_0	3.21E−11	
dx	1.36E−12	
χ2/DoF	R^2	
1.15E−13	1	

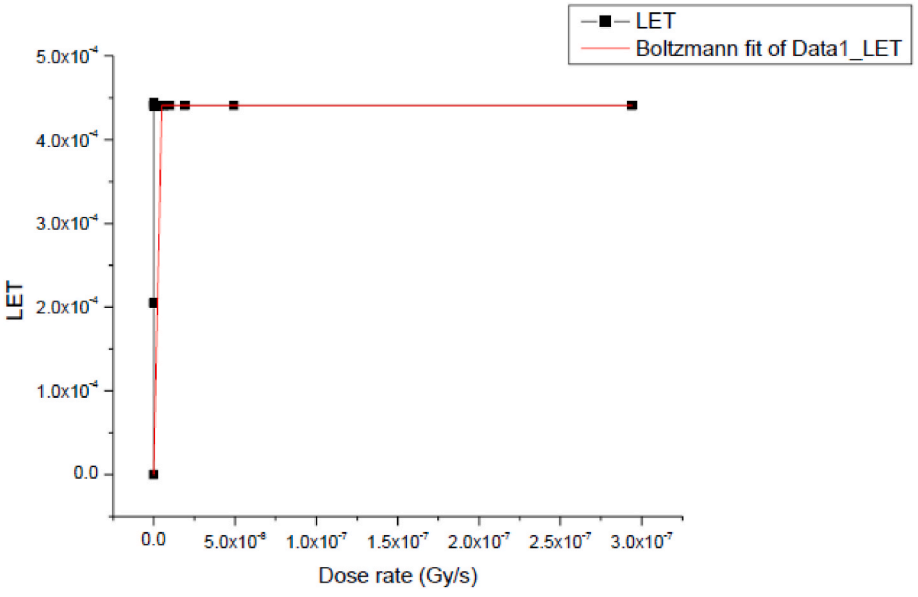


Fig. 8. Dose rate versus LET for radiolysis with β-particles.

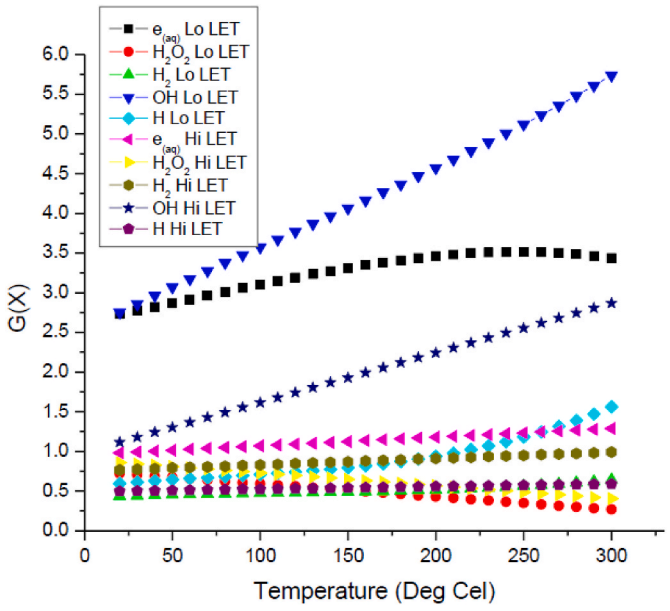


Fig. 9. G-values as functions of temperature.

reduction reaction that occurs in anatomy of the organism. The amount of radiolysis products is regulated by the redox reaction which acts as a catalyst, as shown in the formation of NO in the three-step reaction (Miki, et al., 1995):

$$Fe^{3+} + e^{-}_{aq} \rightarrow Fe^{2+} \quad \text{Eqn 6}$$

$$Fe^{2+} + NO \rightarrow Fe^{2+} - NO \quad \text{Eqn 7}$$

$$NO_2^- + e^-_{aq} \rightarrow N_2^{2-} \underset{H^+}{\rightarrow} NO + OH^- \quad \text{Eqn 8}$$

In these chemical reactions, the Fe^{2+} and e^-_{aq} which are required for step 2 (Eqn (7)) and step 3 (Eqn (8)), respectively, are formed in step 1 (Eqn (6)). The $Fe^{2+} - NO$ in Eqn (7) is an *activated complex* at the top of activation energy (Eshov et al., 2003).

3.3.2. *Implications for material physics*

There are many heavy metal elements that are used in the construction of spent fuel cask, fuel assembly etc which can undergo change in an oxidation state. In addition to Fe, which has already been discussed in the previous section, some of these elements include Mn, Cr, Ni, and U (cf Table 1). Which of these undergo oxidation-reduction (i.e. oxidation or reduction) and whether the process is endothermic or exothermic depends on the, (anode-cathode pair); the electrode potential; and the Gibbs free energy which determines whether the reaction is endothermic or exothermic.

3.3.2.1. Oxidation-reduction of UO_2. Uranium has low solubility in water; however, its solubility at the UO_2/water interface increases significantly because of the α,β, and γ-flux from actinides and fission products which accelerate the dissolution of the UO_2 matrix in water. This dissolution is driven mainly by the oxidation of UO_2 according to the following reaction (Nilsson, 2014; Roth and Jonsson, 2008; Miki et al., 1995; Newton, 1975):

$$UO_2(s) + OX \rightarrow UO_2^{+2}(s) + RED$$
$$UO_2^{2+}(s) \rightarrow UO_2^{2+}(aq) \quad \text{Eqn 9}$$

where OX is an oxidant (oxidising agent) and RED is a reducing agent.

In a geological repository of spent fuel waste there is a potential for the ingress of ground water, where the oxidation process is driven by the formation of soluble complexes in ground water between UO_2^{2+} and HCO_3^{-2}/CO_3^- (Nilsson, 2014). The rate of dissolution of UO_2 in water/UO_2 interface is determined by the concentration of the oxidant $[OX]$, the surface area (SA) of UO_2 in contact with water and the volume (V) of the solution. The relationship among these variables is described mathematically as by Eqn (10) (Roth and Jonsson, 2008; Broudic et al., 2004)

$$-\frac{d[OX]}{dt} = k\frac{SA}{V}[OX] \quad \text{Eqn 10}$$

where k is the reaction rate constant.

Alternatively, in storage conditions where the formation of chemical complexes is not favourable, dissolution will proceed via oxidation with O_2 or H_2O_2. Of the two oxidants, oxidation via H_2O_2 is more important than that via O_2 because it is more than 100 times faster than when oxidation proceeds via O_2. The oxidation process by H_2O_2 is described by Eqn (11) and Eqn (12):

$$UO_2(s) + H_2O_2 \rightarrow OH^{\bullet} + OH^- + UO_2^+(s) \quad \text{Eqn 11}$$

$$OH^{\bullet} + UO_2^+(s) \rightarrow OH^- + UO_2^{2+}(s) \quad \text{Eqn 12}$$

From this (i.e. Eqn (11) and Eqn (12)) it is evident that the dissolution of UO_2 by H_2O_2 results in the yields two radiolysis radical products, $OH^{\bullet}$ and OH^-, which indicates that the yield of one type of radiolysis species is dependent on the presence/existence of other radiolytic species in the solution. The dissolution of UO_2, and eventually the change in matrix structure when exposed to radiation, is related to the radiation dose α,β, and γ-flux from the actinides listed in Tables 2 and 7. In addition, the G-values have been found to be related to α,β, and γ-flux. The interdependence of the rate of dissolution of UO_2 at the water/UO_2 interface, the yield of radiolysis products and the effect of α,β, and γ-flux on the dissolution rate and G-values have been confirmed by Sattonnay et al. after an experimental analysis of leaching of UO_2 after exposure to α-radiation from ^{238}Pu and ^{239}Pu who discovered that the dissolution rate of UO_2 at the water/UO_2 interface was as a result of the redox induced by α-radiolysis (Sattonay et al., 2000; Jegou et al., 2004; Roth and Jonsson, 2008).

3.3.2.2. Oxidation reduction of iron. Iron plays an important role in the radiolysis process. Although is often needed only in small quantities, about 5 ppm, it plays an important role in radiolysis for Fe^{3+} as the oxidising agent. In spent fuel casks iron forms part of the design of the cask in various material compositions such as SS304 (66–75%), borated steel (67%), and cast iron (92.67%), with the % in brackets indicating the fraction of Fe in the compound/alloy (cf Table 1)) (Leotlela, 2016; Radulescu and Gauld, 2011).

The effect of Fe^{2+} in the production of radiolysis products is presented by (Newton, 1975)

$$Fe^{2+} + H_2O_2 \rightarrow Fe^{3+} + OH + OH^- \quad \text{Eqn 13}$$

$$OH + H_2 \rightarrow H_2O + H \quad \text{Eqn 14}$$

$$Fe^{3+} + e^- \rightarrow Fe^{2+} + OH^- \quad \text{Eqn 15}$$

Considering the above equations, i.e., Eqn (13) to Eqn (15), it is noted that Fe^{2+} was only added at the beginning of the reaction and played no role in Eqn (14), and at the end of the chemical reaction process it was released (cf Eqn (15)). The fact that the reaction needed a small quantity (5 ppm) of Fe^{2+} and at the end of the chemical reaction it was ejected unaltered fits well in the description of the role and properties of a catalyst; it is thus a catalyst in the above reaction, serving the purpose of formation of water (H_2O) and hydrogen (H) from the reaction mechanism represented by Eqn (14), and OH^- represented by Eqn (15).

In the study conducted by Grenthe et al. it was discovered that G(H_2) decreased from 0.26 M during the period in which Fe^{2+} was added to 1E-

4 M (Grenthe et al., 1983).

3.3.2.3. The role of zirconium. Zirconium (Zr), which is the cladding material of the UO_2 fuel pellet (cf Table 1), is inactive in water but reacts with it (i.e. with water) to produce ZrO_2 (s) and H_2(g) according to the reaction represented by Eqn (16);

$$Zr(s)+2H_2O \rightarrow ZrO_2(s)+2H_2(g) \quad \text{Eqn 16}$$

Because this reaction is low, there is a high probability it will persist for a long time, increasing the likelihood that it will act as a reducing agent for actinides.

The build-up of actinides such as plutonium, uranium, neptunium and americium, as indicated by Leotlela (2021), not only poses a radiological health risk but also serves a risk of premature failure of structures of a fissile system by acting as excellent oxidation-reducing agent in a redox reaction, thus acting as a catalyst that either lowers or decreases the activation potential of some chemical reactions, subsequently resulting in either a decreased or increased yield of respective free radicals (Newton, 1975).

4. Discussion

The radiation-induced health conditions observed after radiation exposure are the biological effects of exposure to the free-radical by-products of radiolysis that are formed as a result of the ionisation of atoms in a target material (cf to Eqn 17-Eqn (25)) (Leotlela et al., 2020a, b). The fact that the interaction of ionising radiation with matter can lead to either ionisation or excitation is described by Lipinski (2011) and Caer (2011).

If, in the process of interacting with biological matter, the particle transfers a sufficient amount of energy, i.e. $E_{incident\ particle} \geq 13eV$, then the ionisation of H_2O occurs as $\rightsquigarrow \boldsymbol{H_2O}$ (Dzaugis et al., 2015; Elliot et al., 2019). If, however, the projectile does not have sufficient energy to dislodge the electron from the target atom, given that the minimum energy required for ionisation is $\geq$ 7.4, that is, $(E_{threshold\ for\ excitation}) \geq 7.4\text{eV}$, then the electron may only be *excited* to higher energies and not dislodged from the atom as $\rightsquigarrow \boldsymbol{H_2O^*}$.

According to Kabakchi et al. (2013), ionisation or excitation is best optimised if certain chemical conditions for reactants are maintained. Their study discovered that if the temperature (T) of an experimental solution is 65 °C with pH ~ 8, and the energy of the incident particle above the threshold energy for dissociation, i.e. $E_{incident\ particle} \geq 13eV$, H_2O^* will dissociate into $H^{\cdot}$ and $OH^{\cdot}$, as per Eqn (17) (Kabakchi et al., 2013).

$$H_2O^* \rightarrow H^{\bullet} + H^{\bullet} \quad \text{Eqn 17}$$

Alternatively, H_2O^* will dissociate into H_2 and O according to

$$H_2O^* \rightarrow H_2 + O(^1D) \rightarrow H_2O. \quad \text{Eqn 18}$$

The H_2O from Eqn (18) will dissociate into H_2 and 2 $OH^{\cdot}$ as follows:

$$2H_2O \Rightarrow H_2 + 2OH^{\bullet} \quad \text{Eqn 19}$$

The *ionisation* phase will proceed as described by Eqn (20) to Eqn (24).

$$H_2O \xrightarrow{ionisation} H_2O^+ + e^- \quad \text{Eqn 20}$$

$$H_2O^+ \rightarrow H_2O \rightarrow HO^{\bullet} + H_3O^+ \quad \text{Eqn 21}$$

$$H_2O^+ + e^- \rightarrow H_2O \rightarrow HO^{\bullet} + H^- \rightarrow H_2O \rightarrow OH^{\bullet} + H_2 + OH \quad \text{Eqn 22}$$

$$H_2O^+ + e^- \xrightarrow{\text{hydration}} e^-_{aq} \quad \text{Eqn 23}$$

$$H_2O^+ + e^- \rightarrow H_2O^* \quad \text{Eqn 24}$$

The final stage (chemical stage) is summarised by collecting all the end products of the stages depicted by the preceding equations (cf Eqn (25))

$$H_2O \xrightarrow{\text{ionizing radiation}} OH, e^-_{aq}, H, HO_2, H_3O^+, OH^-, H_2O_2 \text{and} H_2 \quad \text{Eqn 25}$$

The results of Kabakchi et al. (2013) were confirmed by Butarbutar et al., in 2014, who reported that they observed the same results using Monte Carlo analysis. In addition, Butarbutar et al. (2014) found that the most important free radicals and molecular radiolysis products are e^-_{aq}, $H^{\bullet}$, $OH^{\bullet}$, H_2 and H_2O_2 (Butarbutar et al., 2014; Caer, 2011). The importance of this finding is based on the following facts:

- e^-_{aq} and $H^{\bullet}$ are strong reducing agents.
- OH^- and H_2O_2 are strong oxidising agents.

This makes them corrosive and, therefore, a potent health risk.

In nuclear facilities such as nuclear reactors and spent fuel storage facilities, energy transfer occurs when fast neutrons undergo thermalisation from a fast energy range to a thermal energy range (cf Eqn (26)), as neutrons undergo scattering among other neutrons and atoms of the target material (Leotlela, 2016; Leotlela et al., 2020a,b).

$$\ln\frac{E_0}{E_n} = n\left[1 + \frac{(A-1)^2}{2A} ln\left(\frac{A-1}{A+1}\right)\right], \quad \text{Eqn 26}$$

where.

A is the mass of the struck nucleus (A = 1 for a proton)
E_0 is the initial neutron kinetic energy, and
E_n is the average energy of the neutron after n individual elastic scattering collisions.

4.1. Relationship between radiation dose, interaction distance, LET and G-value

Analysis of cell damage inflicted by radiation exposure requires knowledge of the underlying causes of the radiation dose and the responses of the cell to the amount of radiation to which it is subjected. This may be ascribed to the following processes/relationships.

4.1.1. LET as a function of the dose rate

The analysis of the relationship between the dose rate and LET showed different responses of the LET to the dose rates for α- and β-exposures.

4.1.1.1. α-Dose rate versus LET. It is evident from the simulation results illustrated in Fig. 4 that for a given target material and α-projectile the response of LET to the dose rate differs, depending on prior radiation exposure and radiation dose received, and can be divided into various stages, which are described below together with their respective (x, y) coordinates in parentheses.

- A (20.001, −0.00217)–B (20.097, 0.13825): The analysis indicates that at this dose rate, LET is highly sensitive to the dose rate, as a small difference in the dose rate results in a rapid increase in LET. This large sensitivity may be attributed to the fact that before radiation exposure, all atoms constituting the media are in the ground state and still have their regular chemical structure with their respective unit cell densities. Because of this, all unit cells are equidistant from one another. However, when a medium is exposed to α-radiation, because of the difference in the atomic sizes of α-particles and those of hydrogen and oxygen in the water molecule, the structure of its unit cell will change (radiation damage). The charge in the α-particle will distort the unit cell even further as the α-particle will be attracted to $O^{\delta-}$ of the water molecule. The energy

transferred is much higher at lower doses than that at higher doses because of (1) the large amount of work that must be done in distorting the original 'pure' structure and (2) high concentration of $O^{\delta-}$ available for the α-particles to attach themselves to.

- B (20.097, 0.13825)–C (20.413, 0.13488): The LET decreases slightly (ΔGy/s = 20.413 − 20.097 = 0.316, ΔLET = 0.13488 − 0.13825 = −0.00337 MeV/μm). This may be ascribed to the fact that the structure of the unit cell has been changed by the previous α-doping process; therefore, the density of the unit cell has decreased, and there are fewer atoms of the medium, posing resistance to the diffusion of α-particles. In addition, the concentration of $O^{\delta-}$ has decreased because of the previous doping process, and the result is, therefore, a slight decrease in LET per dose rate.
- C (20.413, 0.13488)–D (21.633, 0.15119): In this region, LET increases again, albeit at a lower rate than that between A and B. This may mean that because of the previous irradiation, the unit cells have taken on a completely new and permanent structure that has a completely different unit cell density and volume density from what we started with. Because of changes in volume and the structure of the unit cell, there are increases in the interaction rate between the diffusing α-particles and in linear energy transfer.

4.1.1.2. β-Dose rate versus LET. The dose rate of a β-particle is substantially lower than that of an α-particle because of the charge and difference in volume; the β-particle has a single negative charge (−1), whereas the α-particle has a +2 charge. Thus, in consideration of only the charge, the α-particle will exert a much stronger electrostatic force on $O^{\delta-}$ of water than the β-particle does on $H^{\delta+}$; consequently, the α-particle will cause a larger distortion (radiation damage) than that caused by the β-particle. With respect to the atomic sizes of the two particles, the radius of the α-particle is 1.67824(83) femtometres (Krauth et al., 2021), whereas the β-particle has a much smaller radius with the same radius as that of electron which is estimated to be between 1×10^{-18} m and 10^{-15} m (Dhobi, et al., 2020) and, therefore, a much higher penetration power than the α-particle. Because of this, for a given target material, the β-particle will diffuse much easier as it can penetrate the material by occupying interstitial positions without resistance and cause less distortion (radiation damage) to the material, thus transferring less energy per unit path length (LET). The α-particle, by contrast, diffuses by substitution techniques and, therefore causes more radiation damage as it should replace the atom of the target material. Because of that, it causes distortion (radiation damage) to the chemical structure of the target material. Because of this, the β-particle transfers a lower-energy material compared to α-particles. Fig. 8 illustrates the same steep increase in LET as the α-dose rate.

5. Conclusion and outlook

Apart from radiological health risk associated with operating a nuclear radiolysis by charged ionising radiation (α and β) from nuclear plants can be used for hydrogen generation because of high Gvalues from and high energy content of hydrogen. There is therefore a great potential for cogeneration between nuclear energy and hydrogen energy generation at the same time.

Proper design of nanotechnology as catalysts and H_2 storage equipment can great improve the power generation supply as well as curb the contribution to climate change caused by emission of CO_2 gasses.

For both Hi-LET (Fig. 4) and Lo-LET (Fig. 8) radiolysis, there is a lower threshold dose limit for which there will be a steep increase in LET; beyond that dose, the LET will experience a gradual decrease and then increase again, albeit at a much lower rate than that before the lower threshold. Corollary: there is an upper LET limit beyond which a dose rate increase will result in little or no further increase in LET.

Exposure of cell tissue to ionising radiation is not, as such, the cause of the radiation-induced health effects that manifest after exposure to radiation. The real cause of these health effects is exposure to the reducing and/or oxidising agents that present themselves as free radicals. Ionising radiation merely serves as an *initiating event* and the means of *sustaining* the production of free radicals. The stronger the oxidative strength of an oxidising or reducing agent, the more potent that agent is. In the list of radicals given earlier, it was noted that O_2 is the strongest oxidising agent, with a standard electrode potential of +1.23 V, whereas H_2 is midway between the weakest and strongest reducing agents and is an oxidising agent with a standard electrode potential of 0.00 V.

Author statement

MJ Leotlela: Conceptualization, Methodology, Formal analysis, Investigation, Writing - Original Draft, Writing - Review & Editing, Resources, Supervision.

Declaration of competing interest

The authors declare that they have no known competing financial interests or personal relationships that could have appeared to influence the work reported in this paper.

Data availability

No data was used for the research described in the article.

Appendix A. Supplementary data

Supplementary data to this article can be found online at https://doi.org/10.1016/j.radphyschem.2023.111361.

References

Ali, I., Basit, M., 1993. Significance of hydrogen content in fuel combustion. Int. J. Hydrogen Energy 18 (12), 1009–1011.

Ali, I., Imanova, G., Mbianda, X., Alharbi, O., 2022. The Role of Radiation in Water Spitting for Hydrogen Generation. Sustatinable Energy Technologies and Assessment.

Ali, I., et al., 2023. Hydrogen production on nano Al2O3 surface by water splitting using gamma raditaion. Journal of Technol Biotechnology 1186–1191.

Anaconda Inc, 2023. Anaconda Documentation. s.l. Anaconda Inc.

Armstrong, D., et al., 2013. Standard electrode potential involving radicals in acqueous solution: inorganic radicals. Bioinorg. React. Mech. 9, 59–60.

Baiocco, G., Barbieri, S., et al., 2016. The origin of neutron Biological effectiveness as a function of energy. Nature.

Baldacchino, G., Brun, E., Denden, I., R, S.R., K, H., 2019. Importance of radiolytic reactions during high LET irradiation modalities: LET effect, role of O2, and radiosensitization by nanoparticlez. Cancer Nanoparticles 10 (3), 1–21.

Basheer, A., Ali, I., 2019. Water photo splitting for green hydrogen energy by green nanoparticles. Int. J. Hydrogen Energy.

Bielski, B., Cabelli, D., Arudi, R., Ross, A., 2009. Reactivity of H2/O-2 radicals in aquous solution. Physical and chemical reference.

broudic, V., et al., 2004. Application of Chemiluminescence to the Study of Alpha, Beta and Gamma Radiolyses of Water s.l.: s.n.

Buettner, G.R., 1992. The pecking order of free radicals and antioxidants. Arch. Biochem. Biophys. 300 (2), 535–543.

Butarbutar, S., et al., 2014. Modelling the radiolysis of supercritical water by fast neutron:Density Dependence of the yields of primary species at 400deg Celcius. Radiat. Res. 182, 695–704.

Caer, S.L., 2011. *Water Radiolysis: Influence of Oxide Surface on H2 Production Under Ionising Radiation,* s.l.: Water.

Christian, P., Kammer, F.V., Baalousha, M., Hoffmann, T., 2008. Nanoparticle: structure, properties, preparation and behaviour in environmental media. Ecotoxicology.

Dhobi, S.H., et al., 2020. Shape and size of electron are determine by the amount of photon energy incidence on it, 62 (2).

Dzaugis, M., Spivack, A., D'Hondt, S., 2015. A quantitative model of water radiolysis and chemical production rates near radionuclide-containing solids. Radiat. Phys. Chem.

Elliot, A., Chenier, M.P., Ouellette, D., 2019. g-values for gamma irradiation as a function of temperature. Can. J. Chem.

Eshov, B., Gordeev, A., Kelm, M., Janata, E., 2003. Rate constant for the reaction of the H atom with H2O2 in acqoeous solution. Radiation Physisc and Chemistry 613–616.

Ford, E., Hughes, M., Wardman, P., 2001. The Reaction of Superoxide Radical with S. Nitrosoglutathione and Products of it Reductive Heterolysis. *Biological Chemistry*.

Grenthe, I., Puigdomenech, Bruno, J., 1983. The Possible Effects of Alpha and Beta Radiolysis on the Matrix Dissolution of Spent Nuclear Fuel. Department of Inorganic Chemistry, Royal Institute of Technology, Stockholm.

Heera, P., Shanmugam, S., 2015. Nanoparticle characterisation and Application: an overview. International Journal of current microbiology and Applied Sciences 4 (8).
Jawhari, A., 2022. Novel nanomaterial for hydrogen production and storage: evaluating the futurity of graphene/graphene composites in hydrogen energy. Energies.
Jegou, C., Muzeau, V., Broudic, F.J., Bart, J., 2004. Effect of Water Alpha Radiolysis on Spent Nuclear UO2 Matrix Alteration s.l.: s.n.
Kabakchi, S., Arkhipov, O., Lukashenko, 2013. Specific features of the radiolysis of water and aqueous solutions of H2 and O2 by mixed neutron and gamma-radiation with a high portion of the neutron component. High Energy Chem. 47 (4), 147–151.
Katsumura, Y., Sunaryo, G., Hiroishi, D., Ishigure, K., 2020. Radiololysis of Water at Elevated Temperature with Gamma Rays and Fast Neutrons. Tokyo, s.n.
Katz, R., Cucinotta, F., 1991. Rbe vs dose for low doses of HIGH-LET radiations. Health Phys. 60 (5), 717–718.
Kentaro, B., et al., 2021. Quantitative estimation of track segment yields of water radiolysis species under heavy ion around the bragg peak energies using Geant4-DNA. Nature: Sci. Rep. 11 (1524).
Kirkegaard, P.B.E.O.J., 2008. *CHEMSIMUL: A Chemical Kinetics Software package.*, s.l.: Danmarks Tekniske Universitet. Riso National laboratoriet for Baeredygtig Energi.
Kloss, G., 2009. Python data plotting and visualisation extravaganza. Python Pap. Monogr. ume 1.
Krauth, J.J., S, K., A, M.A., A, F.D., A, P., B, F., C, T.-L., C, D.S., D, A.J., D, M., P. F, L.M., B. F. S. G. A. L. G. J. G. T, 2021. Measuring the α-particle charge radius with muonic helium-4 ions. Nature.
Leotlela, M.J., 2016. Criticality safety analysis of the design of spent fuel cask, its manipulation and placement. In: A Lonterm Storage. University of The Witwatersrand, Johannesburg.
Leotlela, M.J., 2019. Methodology for Licensing Burnup Credit in Nuclear Criticality Safety Analysis: A Calculational Basis. Scholar Semantic.
Leotlela, M., 2021. Time-dependent variations in the radiological health impact of an interim spent fuel storage facility. Radiat. Phys. Chem.
Leotlela, M.J., Olifant, T., Petr, I., 2017. Time-dependent variation of the neutron multiplication factor in spent fuel storage. Kerntechnik 82 (6).
Leotlela, M.J., Hadebe, N.D., Petr, I., Sunil, A., 2020a. Prediction of dose rates around the interim spent fuel storage facility. Physics and Chemistry.
Leotlela, M.J., Petr, I., Mathye, A., 2020b. Sensitivity of the neutron multiplication factor to water ingress into a spent fuel cask. Kerntechnik 85 (1), 1–16.
Lipinski, B., 2011. Hydroxyl radical and its scavangers in health and disease. Oxid. Med. Cell. Longev.
Miki, M., Kobayashi, K., Tawaga, S., 1995. Kinetic Behaviour of Nitric Oxide in Biological System Studied by Pulse Radiolysis. JAERI-Conference, Ibaraki.
Najjar, Y., Safadi, M., 2016. The Role of Nanotechnology in Improving the Performance of PEM Fuel Cell in Future Automotive Application. Sustainable Energy Enginnering.
Newton, T., 1975. The Kinetics of the Oxidation-Reduction Reactions of Uranium, Neptunium, Plutonium and Americium. s.l. Los Alamos Scientific Laboratory.
Nilsson, K., 2014. Oxidative Dissolution of Doped UO2 and H2O2 Reactivity towards Oxide Surfaces A Kinetic and Mechanistic Study s.l.:s.n.
Radulescu, G., Gauld, I.C., 2011. STARBUCS: A SCALE Crontrol Module for Automated Criticality Safety Analyses Using Burnup Credit. Oak Ridge National Laboratory, Oak Ridge.
Roth, O., Jonsson, M., 2008. Oxidation of UO2(s) in Aquous Solution. Central European Journal of Chemistry, pp. 1–4.
Sattonay, G., et al., 2000. Alpha-radiolysis effects on UO2 alteration in water. J. Nucl. Mater. 11–19.
Sibery, A., 2020. The Alpha Dose Rate Calculator. University of Bristol, Bristol.
Singh, S., Maura, P., Soni, K., 2023. Nanoparticles, their clasification, types and properties. Int. J. Innovat. Res. Technol.
Tretter, V., et al., 2022. Understanding cellular redox homeostasis: a challenge for precision medicine. Int. J. Mol. Sci.
Yoshikawa, I., Takatsuji, T., Nagano, M., T, J., S Endo, M.H., 2000. RBE-LET relatioships of high LET radiation in Drosophila mutations. Journal of radiation reseach 106–116.